Implementation Techniques for Transcutaneous Carbon Dioxide Monitoring: Approaches for Wearable Smart Health Applications

Tuna B. Tufan, *Graduate Student Member, IEEE*, Lawrence Rhein, and Ulkuhan Guler, *Senior Member, IEEE*

***Abstract*—Wearable smart health applications aim to continuously monitor critical physiological parameters without disrupting patients' daily activities, such as giving a blood sample for lab analysis. For example, the partial pressure of arterial carbon dioxide, the critical indicator of ventilation efficacy reflecting the respiratory and acid-base status of the human body, is measured invasively from the arteries. Therefore, it can momentarily be monitored in a clinical setting when the arterial blood sample is taken. Although a noninvasive surrogate method for estimating the partial pressure of arterial carbon dioxide exists (i.e., transcutaneous carbon dioxide monitoring), it is primarily limited to intensive care units and comes in the form of a large bedside device. Nevertheless, recent advancements in the luminescence sensing field have enabled a promising technology that can be incorporated into a wearable device for the continuous and remote monitoring of ventilation efficacy. In this review, we examine existing and nascent techniques for sensing transcutaneous carbon dioxide and highlight novel wearable transcutaneous carbon dioxide monitors by comparing their performance with the traditional bedside counterparts. We also discuss future directions of transcutaneous carbon dioxide monitoring in next-generation smart health applications.**

***Index Terms*—Respiration parameters, ventilation, arterial carbon dioxide, transcutaneous carbon dioxide, long-term continuous monitoring, noninvasive physiological monitoring, wearables, smart health applications.**

I. Introduction

RESPIRATORY diseases lead to a majority of deaths and disabilities, inflicting a significant worldwide health burden [1]. Since the start of the COVID-19 pandemic, over 700 million cases and more than 6 million deaths have been confirmed worldwide [2]. Asthma, a lifelong respiratory disease, is responsible for more than 3,500 deaths annually in the United States [3]. The ability to continuously monitor the respiration effectiveness of at-risk patients in real time is critical to preventing acute respiratory failure before it becomes a threat.

The accurate diagnosis of respiratory diseases requires a measure of the partial pressure of arterial oxygen (PaO_2) and the arterial partial pressure of carbon dioxide ($PaCO_2$) referred to as blood gases [4]. $PaCO_2$ indicates the efficacy of ventilation, the removal of carbon dioxide from the blood through air exchange in the alveoli, and the acid-based status of the blood [5]. The gold standard for measuring $PaCO_2$ is an arterial blood gas (ABG) analysis [6], [7], [8]. The major drawback of ABG sampling, however, is its invasiveness, accompanied by pain, and its limited ability to provide a brief and selective account of the potentially changing ventilatory status of critically ill patients [9], [10]. Moreover, ABG analysis can be performed in only a clinical setting by care providers. The drawbacks of ABG analysis present an urgent need to develop a technology that continuously tracks $PaCO_2$ remotely and provides relevant and accurate data alerting a care provider to an acute health risk and informing the course of treatment outside a clinical setting [11], [12].

Capnography is a noninvasive surrogate technique that measures the partial pressure of end-tidal carbon dioxide ($PetCO_2$) [13]. To perform this method, patients need to wear a mouthpiece or a nasal cannula, causing discomfort and making it challenging for long-term continuous monitoring outside a clinical setting [14]. Furthermore, recent research suggests that the association between $PetCO_2$ and $PaCO_2$ is not strong enough to provide an accurate assessment of the conditions in individuals with respiratory disorders [15].

Transcutaneous monitoring is a noninvasive method of assessing $PaCO_2$, which measures carbon dioxide (CO_2) diffusing through the skin, that is, transcutaneous CO_2. Changes in transcutaneous CO_2 are directly correlated with changes in arterial CO_2 [16], [17], [18]. Partial pressure of transcutaneous carbon dioxide ($PtcCO_2$) has traditionally been measured by an electrochemical sensing technique [19], [20]. Although conventional electrochemical monitors accurately monitor $PtcCO_2$ [21], [22], the transformation of a conventional monitor into a wearable is hindered by several factors, including i) the calibration mechanism, which requires a gas bottle to correct drift caused by

Manuscript received 9 July 2023; revised 28 August 2023; accepted 28 September 2023. Date of publication 9 October 2023; date of current version 26 February 2024. This work was supported by the National Science Foundation (NSF) under Grant ECCS-2143898. *(Corresponding author: Ulkuhan Guler.)*

Tuna B. Tufan is with the Department of Electrical and Computer Engineering, Worcester Polytechnic Institute, USA.

Lawrence Rhein is with the Department of Pediatrics, UMass Chan Medical School, University of Massachusetts, USA.

Ulkuhan Guler is with the Department of Electrical and Computer Engineering, Worcester Polytechnic Institute, Worcester, MA 01609 USA (e-mail: uguler@wpi.edu).

Digital Object Identifier 10.1109/TBME.2023.3322871

electrochemical materials [23], ii) a heating element, and iii) the use of wet electrodes [12].

Efforts to miniaturize transcutaneous CO_2 monitors have focused on two sensing techniques, the most common of which uses nondispersive infrared (NDIR)-based sensing. This technique, similar to capnography, which measures end-tidal CO_2 [24], entails the use of the infrared (IR) absorption of CO_2 molecules to quantify transcutaneous CO_2. Miniaturized wearable transcutaneous CO_2 monitors in the form of a wristband have been recently tested by several groups [25], [26]. Advancements in luminescent sensing films and optoelectronics have led to the application of the luminescence sensing technique, emerging as the second technique, in miniaturized wearable prototypes for transcutaneous CO_2 monitoring [27], [28], [29]. These prototypes employ sensing films whose luminescence characteristics are sensitive to CO_2.

This article i) presents a review of techniques for sensing transcutaneous CO_2, including electrochemical, NDIR and luminescence sensing, ii) investigates existing and nascent transcutaneous CO_2 monitors presented in the literature, and iii) discusses their features, such as reliability, response time, miniaturization, and wearability for continuous remote monitoring. The organization of this article is as follows. Section II provides the medical relevance of $PaCO_2$ and $PtcCO_2$ sensing, underscoring the importance of $PaCO_2$ in determining a patient's respiratory condition. Section III elaborates on the sensing techniques for transcutaneous CO_2 monitoring. Section IV presents reviews of transcutaneous CO_2 monitors, including both contemporary devices and emerging miniaturized, wearable monitors, and Section V evaluates their suitability for the continuous, remote monitoring of transcutaneous CO_2 in the context of smart health applications. Finally, Section VI presents concluding remarks.

II. Medical Significance of Transcutaneous Carbon Dioxide

The assessment of respiration effectiveness in patients with respiratory diseases is complex, requiring a comprehensive analysis that accounts for multiple oxygenation and ventilation parameters. In current clinical practice, oxygenation is measured by three primary parameters: the arterial saturation of oxygen (SaO_2), that is, the fraction of oxygen-saturated hemoglobin to total hemoglobin; the PaO_2, or unbound free oxygen (O_2) molecules dissolved in plasma; and the arterial O_2 content (CaO_2), or the total number of O_2 molecules. Ventilation is also measured by two primary parameters: the $PaCO_2$, or unbound free CO_2 molecules dissolved in plasma; and the respiration rate. Altogether, these parameters enable a complete assessment of respiration effectiveness as well as blood and tissue oxygenation and lung ventilation.

Although dissolved CO_2 comprises only 5% of the CO_2 present in the blood [30], $PaCO_2$ is a critical blood gas that determines the effectiveness of the pulmonary gas exchange and the acid-base balance in the blood. An abnormal level of $PaCO_2$ indicates either hyperventilation or hypoventilation, that is, increased or reduced ventilation, respectively. Whereas

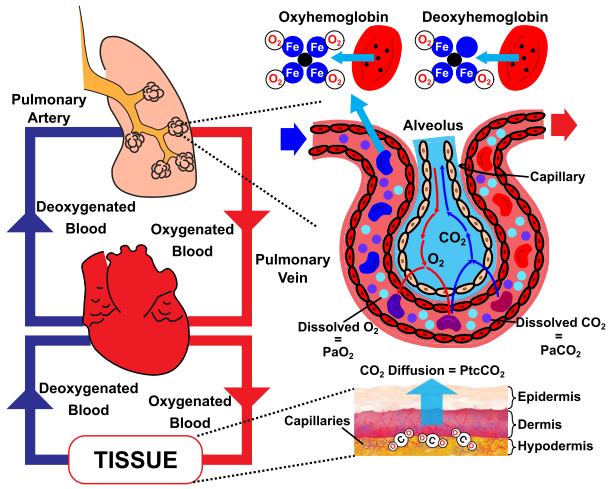

Fig. 1. Diagram of the cardiopulmonary system.

hyperventilation induces hypocapnia, or decreased $PaCO_2$, hypoventilation causes hypercapnia, or increased $PaCO_2$. $PaCO_2$ is the respiratory determinant of the blood potential of hydrogen (pH), together with the metabolic determinant, bicarbonate [31]. Therefore, while hypocapnia leads to respiratory alkalosis, or increased blood pH due to decreased $PaCO_2$, hypercapnia leads to respiratory acidosis, or decreased blood pH due to increased $PaCO_2$ [32]. These respiratory disorders are more likely observed in those with underlying health conditions, including asthma, chronic obstructive pulmonary disease (COPD), and severe obesity [33], [34].

Fig. 1 is a simple illustration of the cardiopulmonary system and the pulmonary gas exchange. The pulmonary gas exchange takes place in the alveoli, in the lungs, where deoxygenated blood is oxygenated by the diffusion of CO_2 from venous blood to the alveoli and O_2 from the alveoli to venous blood. Hemoglobin, a protein found in red blood cells, binds with O_2 in the lungs. Hemoglobin consists of four subunits, each containing an iron atom (Fe) that has the ability to bind with O_2. When O_2 levels are reduced in tissues, oxyhemoglobin releases O_2, enabling its diffusion into neighboring cells. The release of O_2 from hemoglobin is affected by elements such as pH, levels of CO_2, and other molecules. This process facilitates the transfer of O_2 from the lungs to tissues all over the body, where it is utilized for various biological functions.

Abnormal ventilation disturbs the balance in the gas exchange, therefore affecting $PaCO_2$ levels in the capillaries connected to the alveoli and eventually, the capillaries in the entire cardiopulmonary system, including the capillaries in the skin tissue. Transcutaneous CO_2 diffuses from the epidermis through the stratum corneum (the outer layer of the epidermis) into the atmosphere. This phenomena is first observed by Von Gerlach in 1851 through an experiment where he utilized a horse bladder to create an air-filled chamber [35]. He positioned this chamber on his chest for a duration of 24 hours. During this period, Von Gerlach noticed a rise in the concentration of CO_2 within the chamber. Multiple studies [16], [17], [18], one of which is illustrated in Fig. 2 [16], have demonstrated a correlation between

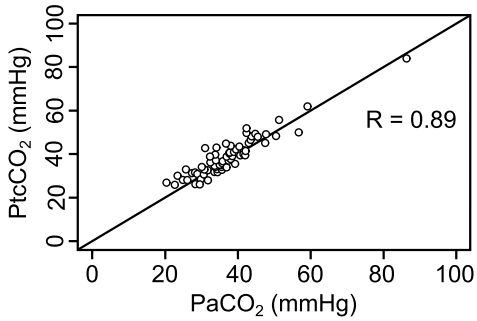

Fig. 2. Linear relationship between $PaCO_2$ and $PtcCO_2$ in a study of children with suspected or confirmed sleep-related respiratory disorders using the Spearman correlation [16].

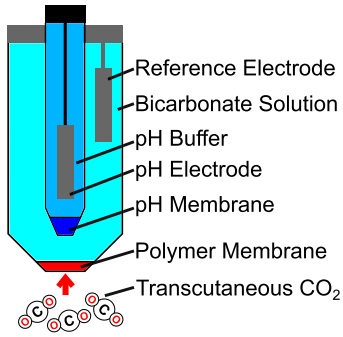

Fig. 3. Simplified diagram of the CO_2-sensitive electrode, which senses the variation in pH resulting from dissolved CO_2 in the electrolyte. Adapted from [40].

$PtcCO_2$ and $PaCO_2$ and indicated that $PtcCO_2$ can be used to estimate $PaCO_2$. The authors measured the $PtcCO_2$ employing a contemporary $PtcCO_2$ monitor [36]. The measurements were taken either from the subjects' forehead or their earlobe after their skin was heated to a temperature of 42 °C.

Healthy individuals are capable of compensating for an increase in $PaCO_2$ levels by increasing their ventilation rate. However, individuals with respiratory muscle fatigue, neuromuscular disorders, obstructive lung disease, obesity, or thoracic cage deformity may experience hypercapnia and hypocapnia. These complications can result in severe conditions, including cardiac rhythm disorders, acute brain injury, and stroke [37]. Continuous long-term monitoring of $PaCO_2$ for individuals with underlying respiratory health conditions would allow the prompt detection of changes and trends in their ventilation status. $PtcCO_2$ measurement, which is both noninvasive and painless, can be performed continuously. Therefore, $PtcCO_2$ monitoring has been gaining traction as a surrogate method for estimating $PaCO_2$ [17], [38], [39].

III. Sensing Principles of Transcutaneous Carbon Dioxide Monitors

Transcutaneous carbon dioxide monitors typically employ a combination of electrochemical and optical technologies. Electrochemical sensors use a gas-permeable membrane to allow CO_2 to diffuse through and react with an electrolyte, generating a measurable electrical signal. Optical sensors, on the other hand, utilize i) infrared light to measure the absorption of CO_2 molecules or ii) luminescence film that reacts to optical excitation and quenches in the presence of CO_2, providing a quantitative assessment. The details of these sensing principles are elaborated in the following subsections.

A. Electrochemical Sensing

The traditional technique for measuring transcutaneous CO_2 is electrochemical sensing, coinvented by Stow and Severinghaus in the 1950s [41]. Stow introduced a design of the first CO_2-sensitive electrode in 1957 [42], and in the following year, Severinghaus improved its electrochemical stability by incorporating sodium bicarbonate into the electrode [19]. The electrodes were initially employed for ABG measurement, but later in 1960, Severinghaus suggested their use for transcutaneous CO_2 sensing [43]. Since that time, the CO_2 electrode has undergone various improvements and transformations, leading to its current form, which is commonly used in conventional bedside $PtcCO_2$ monitors [40], [44], [45], [46].

A diagram of a simplified version of the CO_2-sensitive electrode appears in Fig. 3. The polymer membrane allows CO_2 to diffuse through the electrode, which consists of two compartments, with a pH electrode and a reference electrode. In the first compartment, CO_2 dissolves into a bicarbonate solution, forming carbonic acid (H_2 CO_3), which then dissociates into hydrogen ions (H^+) and bicarbonate (HCO_3^-). The pH membrane in the second compartment detects the resulting change in pH, which in turn affects the potential difference between the pH electrode and the reference electrode. The change in pH is expressed in terms of the partial pressure of CO_2 (PCO_2), based on the Henderson–Hasselbalch equation as follows,

$$pH = pK_a + \log\left(\frac{[HCO_3^-]}{PCO_2}\right), \tag{1}$$

where pK_a is the dissociation equilibrium constant for the dissociation of carbonic acid in water and $[HCO_3^-]$ is the bicarbonate concentration. Since the HCO_3^- solution is highly concentrated, the changes in $[HCO_3{}^-]$ resulting from the dissolved CO_2 can be neglected [45]. Therefore, the measured pH can be expressed as

$$\Delta pH = pK_a - \log(PCO_2), \tag{2}$$

and the measured pH is linearly proportional to $\log(PCO_2)$.

B. Nondispersive Infrared Sensing

NDIR sensors are commonly used for CO_2 sensing for various applications, including environmental and health applications [47], [48], [49], [50]. These sensors operate based on the principle that the IR light transmittance of CO_2 changes at different wavelengths along the spectrum. The highest level of absorption for CO_2 occurs at a wavelength of 4.26 μm. The Beer-Lambert law mathematically expresses the relationship between the absorbance of IR light and the concentration of

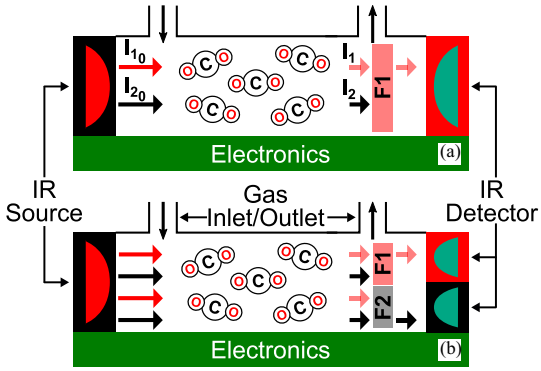

Fig. 4. Diagram of an IR sensor (a) with a single optical band-pass filter (F1) and an IR detector; (b) with an additional filter (F2) and an IR detector as a reference.

CO_2 as

$$Absorbance = \mathcal{E}(\lambda)cl, \tag{3}$$

where $\mathcal{E}$ is the molar absorption coefficient ($M^{-1}\,cm^{-1}$) of CO_2 at wavelength λ, c the molar concentration of CO_2 (M), and l the optical path length (cm) at which the IR light is exposed to CO_2.

Fig. 4 displays a diagram of an NDIR sensor employing the IR absorption principle of CO_2. The system mainly consists of an IR Source, an IR detector, sensing electronics, and a gas cell. Commonly used components for IR sources include IR lamps, IR light-emitting diodes (LEDs), and micro-electromechanical system (MEMS) heaters. Thermopiles, pyroelectric sensors, photoacustic sensors and photodiodes are often employed as IR detectors [51], [52]. The IR source emits light at a wavelength of around 4.26 μm, which overlaps with the absorption spectrum of CO_2, ensuring efficient absorption by CO_2. Other gas molecules present in the measurement medium and the absorption spectra of these gases can also overlap with the emission range of the IR source [51]. For instance, water vapor (H_2 O) has an absorption spectrum in the mid-IR range; during transcutaneous monitoring, the humidity of the skin can cause an accumulation of H_2 O in the measurement medium and affect the performance of the sensor [26]. Thus, an optical band-pass filter (F1) is used before the detector with a passband centered at 4.26 μm, reducing the cross-sensitivity to other gas molecules.

IR radiation transmitted from the source has two components: radiation in the absorption spectrum of CO_2 (I_{1_0}) and radiation outside this spectrum (I_{2_0}). I_{1_0} is absorbed by the CO_2 molecules as it travels to the detector in the gas cell according to (3). The radiation is calculated at a particular wavelength, λ, corresponding to the peak absorption wavelength of CO_2, 4.26 μm. The radiation along the optical path, I_1, is expressed as

$$I_1(\lambda) = I_{1_0}(\lambda)e^{-\mathcal{E}(\lambda)cl}. \tag{4}$$

The absorption of I_{2_0} is not impacted by CO_2 molecules, but rather by other gas molecules such as water molecules that may be present in the gas cell. The radiation outside the absorption spectrum along the optical path is denoted as I_2. At the end of the optical path, the optical band-pass filter, F1, passes only I_1. Hence, the potential contribution of the confounding gas molecules is minimized at the detector end.

Another factor affecting the performance of the sensor is degradation in the source intensity, causing measurement drift. An additional band-pass filter (F2) and a detector can therefore be used, as demonstrated in Fig. 4b, for factoring out this effect. F2 blocks I_1 and passes I_2, which is independent of CO_2 change but proportional to the source intensity. A secondary detector captures I_2, which serves as a reference for the source intensity, and since both sides of the fraction are equally affected, the ratio I_1/I_2 is relative only to the change in CO_2 but unaffected by the change in the source intensity. To avoid interference from other gases, F2 should have a narrow passband.

The sensors illustrated in Fig. 4 are configured such that the IR source and the detector are facing each other. In this case, the optical path length, l, is defined as the straight path from the source to the detector filled with CO_2 molecules. The sensitivity of the CO_2 measurement depends on l, an increase which results in increased exposure to CO_2, therefore yielding a more sensitive measurement [53]. On the other hand, higher absorption due to the longer path length and increased exposure to CO_2 molecules, limits the maximum PCO_2, which can be measured. Therefore, maximum l is determined by the desired PCO_2 range. Increasing the optical path length not only affects the sensitivity and measurement range but also leads to increased sensor size. To increase l effectively and maximize the exposure to the CO_2 molecules, studies have proposed spherical gas cell structures with reflective surfaces [48], [54].

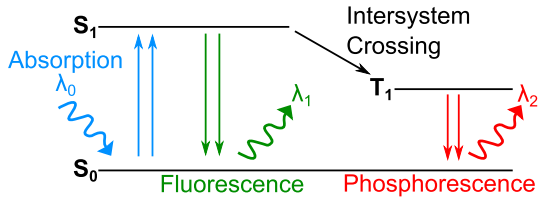

Fig. 5. Simplified Jablonski diagram.

C. Luminescence Sensing

The emission of light from a substance owing to the return of excited electrons to a lower energy state is defined as luminescence [55]. The simplified Jablonski diagram in Fig. 5 illustrates the states of electrons during luminescence. The process involves the absorption of light by a functional group referred to as a luminophore, which excites the electrons in the luminophore from the ground state (S_0) to a higher energy state (S_1). Upon returning to the ground state, the electrons emit photons with a wavelength of λ_1. Alternatively, the electrons may transition to the first triplet state (T_1) and return to the ground state, emitting photons with a wavelength of λ_2. These emissions are referred to as fluorescence and phosphorescence, respectively, and are collectively referred to as luminescence. As absorbed light has higher energy than emitted light, the wavelength of the absorbed light, λ_0, is shorter than the wavelength of the emitted light, λ_1 or λ_2. This difference is known as the Stokes shift [55].

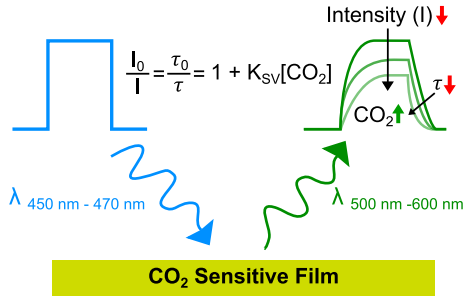

Fig. 6. Relationship between luminescence intensity and lifetime with CO_2 concentration in CO_2-sensitive films.

The intensity and lifetime of luminescence can be reduced by quenching, which occurs when a luminophore interacts with another molecule [55]. In this process, the quencher molecule collides with the excited luminophores, causing them to return to the ground state without emitting a photon. As the concentration of quencher molecules increases, the luminescence intensity and lifetime decrease. The Stern-Volmer equation is used to quantify the kinetics of quenching as follows:

$$\frac{I_0}{I} = \frac{\tau_0}{\tau} = 1 + K_{SV}[Q], \tag{5}$$

where the initial and quenched luminescence intensity are represented by I_0 and I, respectively, and the initial and quenched luminescence lifetime by τ_0 and τ, respectively. The Stern-Volmer constant is denoted by K_{SV} and [Q] represents the concentration of the quencher [55]. CO_2 can quench pH-sensitive luminophores, which can be used to form sensor films that are sensitive to the concentration of CO_2 [56], [57]. A commonly used pH-sensitive luminophore for the construction of CO_2-sensitive luminescent films is 8-hydroxypyrene-1,3,6-trisulfonic acid trisodium salt (HPTS) [58], [59].

Fig. 6 presents an example of a CO_2-sensitive luminescent sensing film excited by a pulse of blue light. The concentration of CO_2 in the environment affects the resulting luminescence; as a result, the CO_2 concentration can be monitored by analyzing changes in the luminescence curve characteristics. The methods for quantifying the luminescence characteristics can be categorized as luminescence intensity, luminescence lifetime, and luminescence ratio. The subsequent subsections provide a detailed explanation of these techniques.

1) Luminescence Intensity: The intensity of luminescence is altered by the concentration of CO_2, as expressed in the Stern-Volmer (5). As the energy of returning electrons is lost during the collision with CO_2 molecules, the intensity of luminescence decreases while the concentration of CO_2 increases, illustrated in Fig. 6. Confounding factors, such as the degradation of the excitation intensity, optical path changes, or the photo-bleaching of the luminescent film, affect the measurements of intensity and lead to measurement errors over time. As a result, intensity-based measurements are not widely favored for applications requiring precise and accurate measurement results.

2) Luminescence Lifetime: The lifetime of luminescence is also altered by the concentration of CO_2, as expressed in the Stern-Volmer (5). The average time that a luminophore spends in an excited state before returning to the ground state is described as the luminescence lifetime, which decreases as CO_2 increases. Luminescence lifetime is inherently insensitive to factors like excitation intensity, photodetector sensitivity which affect measurements of luminescence intensity [60]; therefore, it is a reliable indicator of CO_2 concentration. The lifetimes of the pH-sensitive luminophores used in CO_2 sensing, however, are short, typically in the nanosecond (ns) range [61], so measurements become challenging.

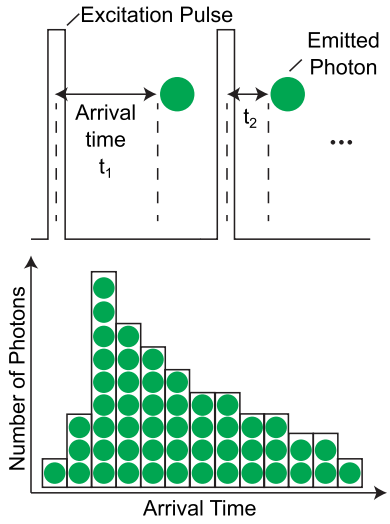

Fig. 7. Time-correlated single-photon counting method.

Time-correlated single-photon counting (TCSPC) is a high-precision method for detecting the short lifetime of luminescent materials [62]. In TCSPC, luminescent material that is repeatedly excited by short pulses emits photons. The objective is to measure the arrival time of these photons by counting the number of photons with the same arrival time, and then creating a histogram (such as that in Fig. 7) that displays the probability distribution of photon arrival times, which relates to the luminescent lifetime, through statistical methods [63]. Since the system is incapable of recording new photons while it is still processing a prior photon event, the primary difficulty with the TCSPC technique is to avoid the accumulation of photons generated by numerous photon emissions occurring within one cycle that go undetected. This duration, when new photons cannot be detected, is known as the detection dead time [64]. Hence, preventing such a pileup and eventually the misrepresentation of the decay time will require the precise adjustment of the detection time with fast optical instruments such as photomultiplier tubes (PMTs) [65]. PMTs are not affected by dead time, but they are large and require high-voltage supplies of hundreds of volts, which significantly increases power consumption [66]. Single-photon avalanche diodes (SPADs) offer a compact option to PMTs; however, even low-power SPAD solutions still require a few watts of power [67], [68].

Another technique for measuring the lifetime of luminescent emissions from the ratio of two equally spaced adjacent areas under the decay curve is rapid lifetime determination (RLD) [69].

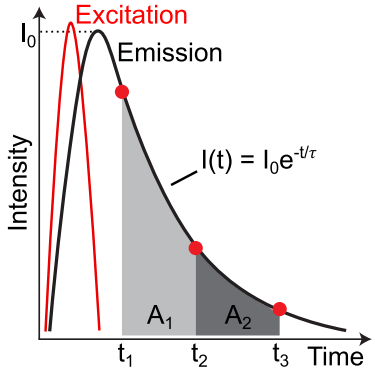

Fig. 8. Rapid lifetime determination method.

Applying RLD, the luminescent material is excited with a short pulse of light. The sampling is performed such that the samples (t_1, t_2, and t_3) divide the area under the curve into two equally spaced areas A_1 and A_2, as shown in Fig. 8. Since the decay curve is a known exponential function [55],

$$I(t) = I_0 e^{(-t/\tau)}, \tag{6}$$

where I_0 is the luminescence intensity right after the excitation and τ is the lifetime, one can calculate areas A_1 and A_2 by using (6) and the samples at t_1, t_2, and t_3. The lifetime τ is then formulated as

$$\tau = \frac{-\Delta t}{ln\frac{A_2}{A_1}}, \tag{7}$$

where Δt is the sampling period ($t_2 - t_1 = t_3 - t_2$). As recovering the decay curve with high resolution is not required, the speed requirements of the readout electronics are relaxed. As the conventional method entails selecting equally spaced integration areas, the sampling points can be chosen according to an optimal scheme for a more accurate calculation of the decay time [70]. An implementation of the RDL technique in application-specific integrated circuits (ASIC) for transcutaneous oxygen monitoring is presented in [71]. To calculate τ, instead of recovering the complete luminescence response, three points from the decay curve were sampled. As the short lifetime of the luminophores necessitates a nanosecond-range sampling rate, the requirement for fast optics and electronics, despite being less strict, still exists.

3) Luminescence Ratio: Another parameter that relates to the concentration of CO_2 in CO_2-sensitive luminescent films is the luminescence ratio. To enable ratio-metric calculation, several methods have been developed, such as leveraging the duality in luminescence characteristics of the luminophore or utilizing multiple excitation sources to illuminate the luminophores. In the following, we elaborate on some of the recent techniques that have been employed.

A recent study that used dual-wavelength excitation found that an HPTS-based CO_2-sensitive film used in a wearable transcutaneous CO_2 sensor overcame the confounding factors [28]. The proposed sensor excites the film by two LEDs with peak wavelengths of 405 nm and 470 nm. When excited at 405 nm, the luminescence response of the film is insensitive to the concentration of CO_2, and at 470 nm, the luminescence intensity decreases as the concentration of CO_2 increases. The ratio of the luminescence response at 470 nm to that at 405 nm minimizes the influence of confounding factors. The 405 nm excitation is used as an isosbestic point to factor out excitation intensity variations and photo-bleaching.

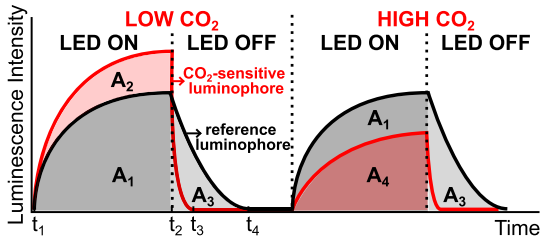

Fig. 9. Time-domain dual lifetime referencing. Adapted from [29].

Another study employed the ratio of protonated and deprotonated emission forms from an HPTS-based CO_2-sensitive film to factor out the confounding factors [59]. By using blue light with a wavelength of 405 nm for excitation, the CO_2-sensitive film emitted light at 455 nm and 515 nm, corresponding to the emissions of the protonated and deprotonated forms, respectively. As the concentration of CO_2 rises, the luminescence intensity of the protonated form shows a corresponding increase, whereas the luminescence intensity of the deprotonated form demonstrates a decrease. Since both forms of luminescence are equally influenced by confounding factors, the ratio of luminescence between these forms provides a measure of CO_2 concentration that remains minimally affected by these factors [72].

A luminescence ratio-based approach called dual lifetime referencing (DLR) can make use of specialized CO_2-sensitive luminescent films containing dual luminophores. Using the DLR technique, researchers presented a miniaturized transcutaneous carbon dioxide monitor that compensates for excitation intensity degradation [29]. The luminescence lifetime of pH-sensitive luminophores such as HPTS is in the range of ns [58]. In the DLR technique, a secondary luminophore, typically Ruthenium(II)-(tris-4,7-diphenyl-1,10-phenanthroline) (Ru(dpp)32+), with a longer lifetime (in the range of microseconds (μ s)), is integrated into the CO_2-sensitive luminescent film with the short-lifetime pH sensitive luminophore [73]. As the long-lifetime luminophore is insensitive to changes in pH and accordingly to CO_2 levels, it acts as a reliable reference luminophore. Both luminophores can be excited by the same wavelength, namely blue light, and their emissions can be detected with a single luminescence detector.

DLR can be applied in two domains: the time domain (tDLR) and the frequency domain (fDLR) [73]. In the tDLR, the luminescent film is excited by a pulse of light, typically by an LED. During excitation, the luminescence of the reference luminophore and the CO_2-sensitive luminophore is A_1 and A_2, respectively. The luminescence of each luminophore is illustrated separately in Fig. 9. After the excitation source is turned off, CO_2-sensitive luminophores decay rapidly in the ns range, and the luminescence of the CO_2-sensitive luminophores

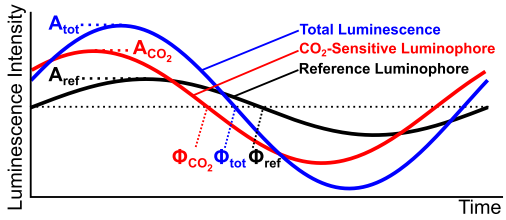

Fig. 10. Frequency-domain dual lifetime referencing. Adapted from [29].

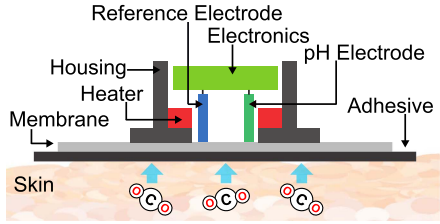

Fig. 11. Simplified schematic of the sensor head in contemporary PtcCO$_2$ monitors.

is negligible ($t_4 - t_2 \gg t_3 - t_2$). Reference luminophores decay in several μ s, generating a luminescence of A_3. When the CO_2 concentration increases during excitation, the luminescence of the CO_2-sensitive luminophores declines to A_4, and luminescence of the CO_2-sensitive luminophores after the excitation is still negligible. The luminescence of the reference luminophore remains constant in both regions (A_1, A_3). Thus, the ratiometric measure of CO_2 at low concentration is defined as the ratio of the total luminescence during excitation to that after excitation,

$$[CO_2]_{low} = \frac{A_1 + A_2}{A_3}, \tag{8}$$

and similarly, at high concentrations, the ratiometric measure of CO_2 is expressed as

$$[CO_2]_{high} = \frac{A_1 + A_4}{A_3}. \tag{9}$$

The dependent factor of CO_2 in (8) and (9) is the luminescence of the CO_2-sensitive luminophore (A_2, A_4) in the numerator. All of the terms (A_1, A_2, A_3, and A_4) respond to changes in the confounding factors, indicating that both sides of the fraction in (8) and (9) vary equally. Therefore, the tDLR method can measure the concentration of CO_2 without being affected by confounding factors.

fDLR applies the same principle in the frequency domain. A sinusoidal wave of blue light excites the luminescent film with two luminophores. The resulting total luminescence (illustrated in Fig. 10), which has the reference and CO_2-sensitive components, is formulized as

$$A_{tot}.\cos\Phi_{tot} = A_{ref}.\cos\Phi_{ref} + A_{CO_2}.\cos\Phi_{CO_2}, \tag{10}$$

$$A_{tot}.\sin\Phi_{tot} = A_{ref}.\sin\Phi_{ref} + A_{CO_2}.\sin\Phi_{CO_2}, \tag{11}$$

where A_{tot}, A_{ref}, and A_{CO_2} denote the peak amplitudes of the total, reference, and CO_2-sensitive luminescence, respectively. ϕ_{tot}, ϕ_{ref}, and ϕ_{CO_2} are the phase of total, reference, and CO_2-sensitive luminescence, respectively. Since the lifetime of the CO_2-sensitive luminophores is within the ns range, the phase shift in CO_2-sensitive luminescence is negligible, that is, $\Phi_{CO_2} = 0$, compared to the kHz or slower range excitation frequency [74]. Hence, if the excitation frequency is sufficiently slow, (10) and (11) are simplified to

$$A_{tot}.\cos\Phi_{tot} = A_{ref}.\cos\Phi_{ref} + A_{CO_2}, \tag{12}$$

$$A_{tot}.\sin\Phi_{tot} = A_{ref}.\sin\Phi_{ref}, \tag{13}$$

ϕ_{ref} is constant, A_{ref} does not change with the concentration of CO_2, however, is sensitive to the excitation intensity, photobleaching, and so on. Therefore, $\cot\phi_{tot}$ yields a ratiometric measure of the concentration of CO_2 that is insensitive to confounding factors,

$$\frac{A_{tot}.\cos\Phi_{tot}}{A_{tot}.\sin\Phi_{tot}} = cot\Phi_{tot} = cot\Phi_{ref} + \frac{1}{\sin\Phi_{ref}}.\frac{A_{CO_2}}{A_{ref}}. \tag{14}$$

While the DLR technique is a new concept in transcutaneous carbon dioxide monitoring, it has been used since early 2000 s for measuring CO_2 and pH in oceanography studies [75], the fluorescent pH imaging [76], monitoring CO_2 in adipose tissue [58], developing chloride optical sensors [77], and imaging intracellular chloride concentrations [78].

IV. Transcutaneous Carbon Dioxide Monitors

In this section, we explore contemporary and emerging transcutaneous carbon dioxide monitors. With the need for noninvasive monitoring, contemporary monitors offer great potential in accurately assessing CO_2 levels in various clinical settings. Moreover, we examine the latest developments in PtcCO$_2$ monitors, focusing on advancements in technology through innovative sensor designs and the integration of electronics and sensors. By examining the current landscape of PtcCO$_2$ monitors, we aim to shed light on the capabilities and challenges of contemporary sensors as well as provide insights into the cutting-edge features and capabilities of modern PtcCO$_2$ monitors.

A. Contemporary Monitors

1) Electrochemical-Based Monitors: Contemporary monitors utilize electrochemical-based sensing, namely CO_2 electrodes, to sense PtcCO$_2$. The electrodes and peripheral components typically fit into a sensor head attached to the subject's skin. A typical sensor head is illustrated in Fig. 11. The sensor head goes into an adhesive attachment ring that allows the placement of the sensor on the skin and isolates the gas exchange from an external environment. The surface of the sensor is directly attached to the skin and CO_2 diffused from the skin passes through a permeable hydrophobic CO_2 membrane. The CO_2 electrodes measure the PtcCO$_2$ as described in Section III-A. A heater integrated into the sensor head increases the local skin temperature to 44 °C, increasing the blood flow rate and local CO_2 diffusion, which improves the correlation between PaCO$_2$ and PtcCO$_2$ [79], [80]. Temperature sensors are deployed in the

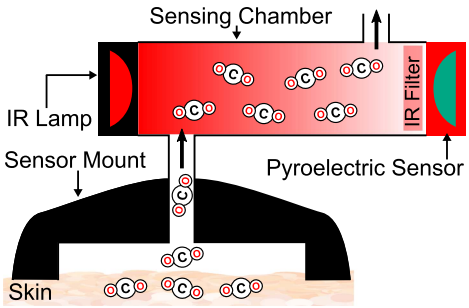

Fig. 12. Proposed NDIR-based $PtcCO_2$ monitor in [82].

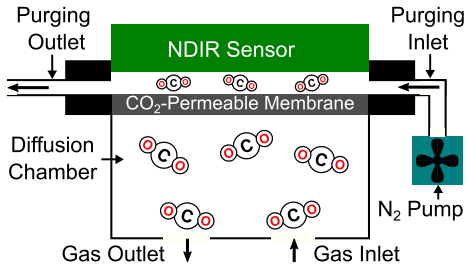

Fig. 13. Schematic of the benchtop experimental setup for the rate-based measurement of the PCO_2. Adapted from [26].

sensor head to provide feedback to the heater for regulating the local skin temperature and for correcting measurement drifts caused by the change in temperature. The electronics in the sensor head digitize the measurement data and transmit the data to a bedside monitor via a wired connection for display [23].

Contemporary monitors, used in clinical settings such as intensive care units (ICUs) or sleep units, provide accurate readings of $PtcCO_2$ that can be used in the estimation of $PaCO_2$ [16], [17]. The accuracy of contemporary monitors relies on sensor calibration that occurs every 12 hrs [46]. Calibrating sensors, required for correcting measurement drift in the electrodes, requires the use of a special gas stored in a separate unit located in the bedside monitor. During this process, the sensor, which must be attached to the calibration unit, is exposed to known PCO_2 to perform one-point calibration.

Typically the sensor response time is about 1–5 minutes [81]. When the sensor head is first attached to the skin, however, it may take up to 20 minutes, with elevated temperatures to $\sim 44\,^{\circ}C$, for the $PtcCO_2$ to reach a state of equilibrium at the interface between the skin and the sensor, lengthening the stabilization time [38]. Despite the miniaturized size of the sensor head, comparable to that of a fingertip, it is still wired to the bedside monitor, so the entire system is portable but not wearable.

B. Emerging Wearable Monitors

1) NDIR-Based Monitors: A broad range of applications in the automotive industry [83], air quality monitoring [84], breath analysis, and capnography devices [24], [53] entail NDIR-based sensing for monitoring CO_2 levels. Recently, several research groups have proposed NDIR-based sensing for transcutaneous CO_2 monitoring [25], [26], [49], [82], [85], mainly to overcome the drawbacks of traditional electrochemical-based sensing discussed in Section IV-A, such as the necessity of frequent calibration with a gas bottle for accurate and drift-free measurements and slow response time of the sensor.

Mainstream capnographs measure CO_2 levels in a patient's airway by placing the NDIR sensor on the airway within the endotracheal tube [24]. Researchers in [82] has adapted this technology to transcutaneous CO_2 monitoring by mounting NDIR sensors on a patient's skin, illustrated in Fig. 12. CO_2 diffusing through the skin is passed through a photoreaction chamber where the partial pressure of CO_2 is measured with NDIR-based sensing. On one end of the photoreaction chamber, an IR lamp is employed as the source, and on the detector side, a pyroelectric sensor and an IR bandpass filter are used. In this implementation, however, the time it takes for the PCO_2 to reach equilibrium slows down the response of the sensor. The diffusion rate of CO_2 from the skin is limited, and even with the addition of a heating element, equilibrium may still take 15–20 minutes to reach, depending on the size of the measurement chamber, skin thickness, and temperature [86].

A study in [26] presents a wearable NDIR-based transcutaneous CO_2 monitor in the form of a wristband. The authors proposed a rate-based measurement method described in [86] for the benchtop experiments. Fig. 13 displays a schematic of the rate-based measurement system in which the NDIR sensor measures the rate of change in the PCO_2 in the diffusion chamber instead of the equilibrium (steady state) value. The rate of change, which is linearly proportional to the PCO_2, can be used to assess the partial pressure in seconds, eliminating the delay of several minutes for the partial pressure to reach equilibrium, which significantly improves the response time of the first reading.

For rate-based measurement, CO_2 in the diffusion chamber must be purged with nitrogen (N_2) before each measurement, The N_2 pump for purging increases the power consumption and the size of the wearable device, while also introducing various complexities in its mechanical structure. Therefore, the authors removed the N_2 pump and the purging mechanism in the wearable device used in subject tests and measured the equilibrium PCO_2 [26]. A polydimethylsiloxane (PDMS) membrane that was both hydrophobic and CO_2 permeable, is used in between the skin and the NDIR sensor to avoid humidity interference. Although the response time remained unchanged, the wearable $PtcCO_2$ monitor utilizing NDIR technology successfully measured PCO_2 for 4.5 hours without requiring additional calibration, following the initial calibration against a commercial breath analyzer.

Another study proposed a thermo-fluidic channel that entailed the use of convection to remove CO_2 from the measurement cell without an external purging system [25]. Fig. 14 illustrates the principle of the proposed thermo-fluidic channel through which blood CO_2 in the gas phase diffuses from the skin as transcutaneous CO_2. To increase the local diffusion rate of transcutaneous CO_2, the skin is heated up to $42\,^{\circ}C$. Cold air from the outside diffuses into the collection cell, where it meets the CO_2. Then the cold air heats up and, along with CO_2 molecules,

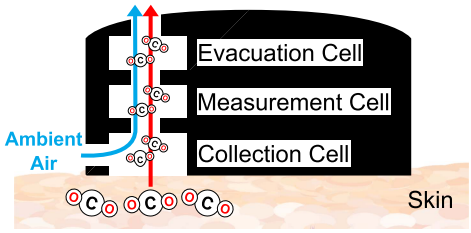

Fig. 14. Thermo-fluidic channel structure employed for the transport of transcutaneous CO_2 in a wristband-based $PtcCO_2$ monitoring device. Modified from [25].

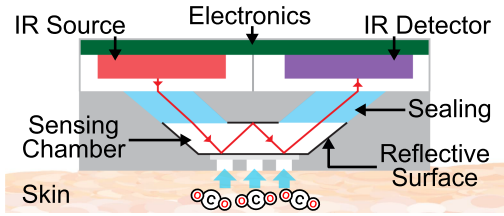

Fig. 15. Miniaturized sensing chamber design for an NDIR $PtcCO_2$ sensor. Adapted from [87]. .

it rises to the measurement cell via the convection principle. Before the air is introduced to the collection cell, however, the authors measure the PCO_2 present in the ambient air in a separate measurement cell in order to prevent measurement errors [49]. The measured CO_2 is released through an evacuation cell, again via convection, to the ambient air so that the CO_2 in the measurement cell circulates without the need for an external pump.

In the measurement cell $PtcCO_2$ is measured with NDIR-based sensing. Two thermopile sensors that detect radiation, each with optical filters of peak transmittivity of 4.26 μm and 3.91 μm, pass the CO_2-sensitive and reference wavelengths. The reference wavelength is utilized to factor out confounding gases that are present in the measurement cell as explained in Section III-B. The reference wavelength is selected as 3.91 μm to ensure minimum water absorption and prevent interference of humidity, therefore to avoid the interference of humidity with the measurements. Another confounding factor that can affect the CO_2 readings is the ambient temperature as the thermopile sensors are not only sensitive IR but also to temperature. Hence, the baseline reading of the thermopile sensors is periodically recorded when the IR source is off to compensate for the ambient temperature affect. Potential affect of a pressure change is taken into account with MEMS pressure sensors integrated into the measurement system.

The authors define a linear-quadratic model for the measurement system for the post-processing of the measurement results and relating $PtcCO_2$ to the blood CO_2. The proposed thermo-fluidic channel is implemented in a wristband to monitor the partial pressure of CO_2 in human subject tests. The wristband monitor detects hypocapnia and hypercapnia conditions after the post-processing of the measurement results [49]. The proposed thermo-fluidic channel reduces the components required for circulating the CO_2 in the measurement cell and enables the miniaturization of the wearable monitor.

The time it takes for the partial pressure of CO_2 to reach equilibrium determines the response time of NDIR sensors, which is inversely proportional to the volume occupied by CO_2 in the sensor. Hence, the response time can be reduced by minimizing the volume of the sensing chamber. A study in [87] presents a miniaturized sensing chamber design that reduces the equilibrium time. The chamber design illustrated in Fig. 15 incorporates reflective surfaces, which are employed to maintain the optical path of IR radiation while minimizing the size of the sensing chamber. This approach enables a reduction in response time without compromising the sensitivity of the sensor. Additionally, the utilization of reflective surfaces reduces the amount of radiation absorbed by the sensing chamber and enhances power efficiency [88].

The circuitry for NDIR-based transcutaneous CO_2 monitors is composed of two main blocks: source-side and detector-side. On the former, the IR source is typically driven by periodic pulses at a frequency as low as 5 Hz, which is fast enough to capture the real-time $PtcCO_2$ variation in humans [49], [85], [88]. The pulses can also be duty-cycled to reduce power consumption [85], and the pulsed operation reduces thermal drift by allowing the IR detectors time to cool off. Pulses can be generated with a low-dropout regulator modulated by a microcontroller [88] or a voltage-controlled pulse width modulator [85]. If necessary, the pulse generator can be coupled with a current amplifier to produce the high current (100–150 mA) required by the IR source [85].

2) Luminescence-Based Monitors: Although luminescence-based sensing has been used for CO_2 measurements in a wide range of applications from oceanography [75] to biology [89], it is a new concept in transcutaneous CO_2 monitoring. Sensor films, described in Section III-C, have several features that benefit transcutaneous monitoring such as the small size of the sensor (as small as 500 μm in diameter and several μm in thickness [90]) and sensor's response times in the range of several seconds [91], [92].

A miniaturized transcutaneous CO_2 monitoring prototype based on luminescence sensing is demonstrated in [27]. The CO_2-sensitive luminescent sensor used in this prototype emits green light (520 nm) when it is excited by blue light (470 nm), and the intensity of luminescence is inversely proportional to the PCO_2. A microcontroller driving a blue LED sends excitation pulses to the luminescent sensor, and a green light-sensitive photodiode captures the luminescence. The photodiode current corresponding to the luminescence yield is amplified by a transimpedance amplifier, the output of which is proportional to the luminescence intensity, used to monitor the CO_2 level. The performance of the prototype is validated by in-vitro experiments. In these experiments, the PCO_2 in a 0–75 mmHg range, which covers the typical $PtcCO_2$ values in humans, is measured successfully. The downside of the sensor is that it must be kept in a saline solution for chemical stability, which can complicate the design of the wearable transcutaneous monitor. Fig. 16 depicts a conceptual model that showcases a wearable device of smart-watch size, containing all the necessary components. The PDMS is proposed to be used in the flexible membrane

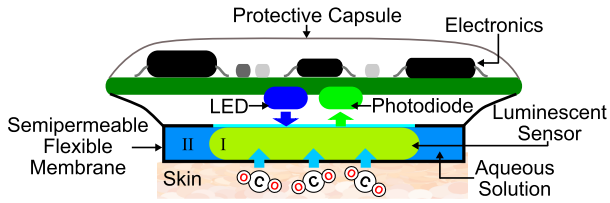

Fig. 16. Miniaturized luminescent film-based transcutaneous CO_2 monitor [27].

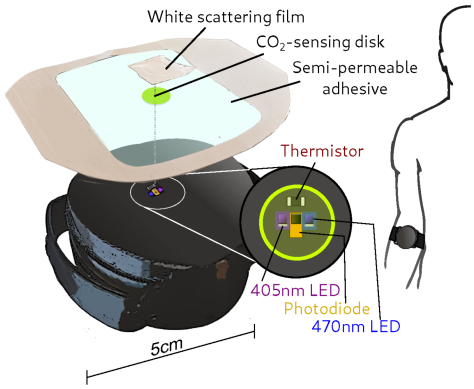

Fig. 17. Wearable transcutaneous CO_2 monitor with a multilayer luminescent sensor and dual-wavelength excitation [28].

design that is impermeable to the saline solution and permeable to CO_2.

The intensity of luminescence can be affected by changes in the intensity of excitation, as mentioned in Section III-C, leading to incorrect $PtcCO_2$ readings in transcutaneous monitors that rely on intensity-based measurement. To account for changes in the excitation intensity, the authors of one study [28] implemented dual-wavelength excitation on a transcutaneous CO_2 monitoring wearable. They used two LEDs with peak emission wavelengths of 405 and 470 nm to consecutively excite a multilayer CO_2 sensor composed of a breathable and scattering silicone film, a polymethyl methacrylate (PPMA)-based film, and a transparent semipermeable film. The study found that luminescence triggered by 470 nm excitation varied with the PCO_2 in the 0–50 mmHg range while luminescence triggered by 405 nm excitation was insensitive to the PCO_2. Both luminescent responses, in the range of 520–530 nm, were captured by the same photodiode with a 500 nm long-pass filter to block excitation wavelengths. The ratio of the luminescent responses yielded a measure of PCO_2, which is insensitive to not only excitation intensity variation but also other confounding factors such as photo-bleaching and motion artifacts. To ensure accurate measurements, the study entailed a 5-minute pre-calibration of the monitor. During this process, the authors fit the acquired values to a predetermined model that described the correlation between the luminescence ratio and PCO_2. The complete system design fit into a wristband with a diameter of 5 cm, shown in Fig. 17. The wristband monitor supports Wi-Fi for the wireless transmission of the PCO_2 values to a personal computer (PC).

A study using the t-DLR method for $PtcCO_2$ monitoring [29] also addresses discrepancies resulting from changes in the excitation intensity. As a result of a single excitation of 465 nm, the sensor film used in this study had peak emissions of 505 nm and 600 nm, corresponding to the emissions of CO_2-sensitive and reference luminophores, respectively. To emulate changes in the excitation intensity, the authors used 60 and 80 mA LED drive currents to excite the sensor; the measurement results from the two scenarios matched in the t-DLR method with a maximum deviation of about 1.6% while the results based on luminescence intensity measurements showed a mismatch of about a 9.5% maximum variation.

The $PtcCO_2$ monitor, which was initially developed by the authors of [29], was further reduced in size and incorporated into a wrist-band wearable in [39]. The wearable was tested on a human subject at two different body sites, the forearm and the fingertip. The response time of the sensor was only about 5 minutes for a 10% CO_2 change during benchtop gas experiments; measurements on the skin, however, indicated that it takes around 25–30 minutes for the PCO_2 in the skin/sensor interface to equilibrate initially. The sensor was also found to require recalibration every 12 hours to correct measurement drift.

Luminescence lifetime is invariant to excitation intensity or photodetector sensitivity changes [99]. To date, nevertheless, lifetime-based measurement has not been used in transcutaneous CO_2 monitors, mainly because the methods listed in Section III-C for detecting ns range lifetimes, namely TCSPC and RLD, require high-speed, complex electronics and optical designs [64]. The limitations in bandwidth prevent analog transient measurement of the luminescence decay curve from meeting the speed requirement. [100]. To achieve ns resolution, one must use single photon detectors such as PMTs and avalanche photodiodes (APDs). Although these detectors have short rise/fall time (typically around several hundreds of picoseconds), they require a high reverse bias voltage (0.1–1 kV) to achieve multiplication factors that yield signal outputs detectable by electronics following the photon detector [101]. This requirement presents a significant challenge in the design of a miniaturized wearable device based on the TCSPC method. These detectors are combined with timing electronics, traditionally a time-to-amplitude converter [100], and contemporary time-to-digital converters with a picosecond-range resolution [102], [103]. Nevertheless, recent developments in miniaturized SPAD-based image sensors offers promising solutions to the challenges of photon counting related to size and power consumption [104]. These fully on-chip image sensors, are presently employed in fluorescence microendoscopy but have the potential for future applications in measuring luminescence lifetime.

V. Challenges and Future Directions

The physical aspects of transcutaneous CO_2 monitors such as size, comfort, and wearability, as well as functional aspects such as accuracy, calibration interval, and response time, along with power consumption, are crucial because the devices enable

TABLE I
COMPARISON OF TRANSCUTANEOUS CO_2 MONITORS

	Electrochemical-Based	NDIR-Based	Luminescence-Based
Device Type	Bedside monitor	Wearable	Wearable
Sensors	CO_2-sensitive electrode	Pyroelectric or Thermopile	CO_2-sensitive film and PIN PD*
Size	mm scale	cm scale	mm scale
Response Time†	Minutes	Seconds	Seconds
Settlement Time‡	~20 min	~30 min	~30 min
Heating	Yes	No**	No
Calibration Period	12 h	8 d	12 h
Power Consumption	10^0-10^3 mW	10^0-10^2 mW	10^1-10^2 mW
Wireless operation	Not available	Available	Available
Maintenance	Moderate	Easy	Easy
Pros	Accuracy demonstrated with clinical tests	Long-term operation without calibration	Small sensor size and fast response time
Cons	Designed as a bedside monitor	Challenging to miniaturize the measurement cell	Photobleaching causes measurement drift
References	[20], [23], [40], [46], [93], [94] [9], [22], [95]–[97]	[25], [26], [85], [98]	[27]–[29], [39], [92]

* PD: Photodiode. ** [25] employs a heating element. †Sensor Response Time. ‡Measurement Settlement Time.

more prolific and versatile monitoring of patients with respiratory diseases in real time outside of a clinical setting [105]. Various aspects of electrochemical-, NDIR-, and luminescence-based monitors are summarized and compared in Table I. The following subsections provide a discussion of the features of each.

A. Device Size

Since wearable monitors, unlike stationary bedside counterparts, enable individuals to carry out regular tasks without being confined to a bed, the ease with which a $PtcCO_2$ monitor can be worn is a crucial factor. The size of the sensor head for electrochemical-based monitors, which include CO_2-sensitive electrodes and required electronics for sensor front-end and data processing, can be as small as 14 mm × 9 mm [23], [93]. Nevertheless, as these monitors are mainly intended for use in clinical settings as bedside monitors, they come equipped with a separate device for displaying data and calibrating the sensor. Aside from the gas bottle within the calibration unit, which hinders the miniaturization of electrochemical-based monitors, the existence of the heating element demanding power outputs in the range of several hundred milliwatts to achieve a skin temperature of 44 °C necessitates the incorporation of large, high-capacity batteries [23], [93]. NDIR-based monitors can achieve greater sensitivity by increasing the optical path between the IR source and the sensor [53]. Therefore, the sensor component of these monitors, which measure several centimeters, are typically larger than that of electrochemical-based monitors. Most NDIR-based monitors, however, can fit in a wearable in the form of a relatively large wristband [25], [26]. Owing to the small size of the sensor in luminescence-based monitors, typically on the order of millimeters, they are well-suited for use in wearable applications, such as watches or patches [28], [39].

B. Response and Initial Settlement Time

Electrochemical-based monitors have a sensor response time that typically falls within a few minutes, determined by the rate of chemical reactions that occur in the electrode [23], [40]. CO_2-sensitive electrodes present a tradeoff between sensitivity and response time, as well as between stability and response time. When a spacer is placed between the polymer membrane and the HCO_3^- solution in the electrode, the measurement sensitivity is enhanced, but the response time also increases. Likewise, a high concentration of HCO_3^- improves the stability of the electrode; however, it also slows down its response [20]. NDIR- and luminescence-based monitors exhibit faster sensor response times, typically in the range of tens of seconds [26], [92].

It is important to note that the reported sensor response time is measured after the CO_2 concentration has reached equilibrium which occurs during the initial settlement time in the measurement medium. In the case of electrochemical-based monitors, it has been observed that the initial settlement time typically lasts approximately 20 minutes [94]. Heating is employed in these monitors to enhance the diffusion rate of CO_2 through the skin, thereby improving the initial settlement time of the monitor. NDIR- and luminescence-based monitors, without the application of heating, report an initial settlement time of approximately 30 minutes [26], [39], whereas for electrochemical-based monitors without heating, the reported initial settlement time is approximately 85 minutes [94]. Using the rate of change in PCO_2 as a measurement instead of the concentration at equilibrium leads to a faster initial measurement. A design that incorporates extra components such as an N_2 pump to implement the rate-based approach increases the size of the device significantly [26], [86]. Conversely, one that includes a measurement medium with a thermofluidic channel eliminates the need for an N_2 pump, allowing the rate-based approach to be implemented in a miniaturized wearable [25].

The response time of a transcutaneous carbon dioxide sensor is crucial for one-time measurements, particularly in rate-based monitors. However, in continuous measurements, it is important to recognize that once the measurement medium within the sensor reaches equilibrium, the overall device's response will mainly depend on the sensor's response time. As a result, the device's response to changes is typically faster than the time it takes to reach equilibrium. Therefore, it is important to differentiate between the settlement time of the device and the sensor's response time in continuous measurement scenarios.

C. Calibration Period

Another crucial element that can impact the performance of a $PtcCO_2$ monitor during continuous measurements over a long period is known as measurement drift. The Food and Drug Administration's instructions on $PtcCO_2$ monitors state that any changes or shifts in $PtcCO_2$ readings should not surpass 10% of the initial reading during the calibration period [106]. For electrochemical- and luminescence-based $PtcCO_2$ monitors, this period is typically 12 hours [39], [46]. Luminescence-based monitors experience measurement drift as a result of the photobleaching of the CO_2-sensitive film. Once photobleached, the film must be substituted. To avoid the need for frequent film replacement, a feasible approach is to decrease the sampling rate of the monitor, thus prolonging the calibration period. As physiological changes in the human body occur slowly, the sampling rate can be as infrequent as 2 samples per minute [39]. However, it is worth noting that CO_2-sensitive luminescence films have not yet reached their full maturity. As the field continues to advance, there is potential for reduced drift in these sensors, similar to what has been achieved with O_2-sensitive luminescence films [60], $\sim$4% in 125 hours. NDIR-based monitors have a longer calibration period than electrochemical- and luminescence-based monitors, which do not involve any chemical process. The zero point of the sensor, however, still needs regular calibration to ensure long-term stability, which is usually achieved using the built-in auto-calibration process [26]. This process uses the default CO_2 concentration of fresh air to calibrate the sensor.

D. Power Consumption

Another important parameter for remote wearable devices is power consumption, which should be minimized to enable long-term, battery-powered operation. Electrochemical-based monitors, however, are primarily designed for bedside use and are usually connected to the main power source. The power consumption of these monitors varies from a few mW to hundreds of mW, which is determined by the heating element's power and the brightness of the display on the bedside monitor [23], [93]. The IR source, the main consumer of power in NDIR-based monitors, usually requires a drive current of 100–150 mA, however by using duty cycling on the source drive signal, the power consumption can be maintained below 100 mW and even reach as low as 3.3 mW [26], [85]. Luminescence-based monitors typically consume tens of mW [27], [39]. It is worth mentioning that the luminescence-based monitors presented in the literature are considered proof-of-concept devices, indicating that there is potential for enhancing their power efficiency.

E. Wireless Operation

For a complete wearable design, the monitoring data should be transferred wirelessly to a personal computer or a mobile device. Current electrochemical-based monitors typically come with a bedside monitor for data visualization that is connected directly to the sensing electrode via wires. NDIR and luminescence-based sensors, however, are still primarily in the development stage and as of now, although a few offer a complete wearable solution using WiFi [28] or Bluetooth Low Energy (BLE) [25] for data transfer, most do not.

F. Motion Artifacts

Motion artifacts can impact the accuracy and reliability of nearly all wearable monitors to some extent [107]. In the case of contemporary monitors, it is crucial that the sensor electrode makes a tightly sealed connection with the skin. If the patient moves excessively, this connection can be disturbed, leading to changes in the balance of $PtcCO_2$ between the sensor and the skin due to the sudden surge of ambient air. Hence, when utilizing these monitors, patients are recommended to remain stationary while the measurement is conducted, ensuring precise readings [23]. This necessity for a secure skin connection also pertains to NDIR and luminescence-based monitors, consequently causing similar effects of motion artifacts on these devices. As there is no requirement for frequent sensor attachment and detachment in long-term monitoring applications, these wearable devices can incorporate more robust adhesives to establish an airtight connection with the skin.

Motion artifacts can also lead to alterations in the optical path, such as displacing the light source or the receiver. These changes have the potential to cause variations in the excitation intensity within monitors that rely on NDIR and luminescence principles. However, luminescence-based monitors that rely on measuring luminescence lifetime or ratio, which are resilient against variations in excitation intensity, could minimize the influence of motion artifacts on alterations in the optical path [39], [60]. The influence of motion artifacts can be assessed by employing a motion sensor, like an integrated accelerometer, within monitors [108]. This sensor can be utilized to establish a connection between the motion artifacts and the discrepancies in the measurements, subsequently addressing the effects of motion artifacts through the implementation of correction algorithms. It is important to highlight that prior investigations into the mitigation of motion artifacts, particularly in wearable photoplethysmography (PPG) sensors, have revealed the difficulty of fully eliminating the influence of motion artifacts [109].

G. Individual Variations

The performance of transcutaneous CO_2 monitors can differ among individuals. This is due to the susceptibility of transcutaneous measurements to the diverse characteristics of individuals' skin. The outermost skin layer, referred to as the

stratum corneum, acts as a barrier that controls the exchange of molecules between the body and the surroundings. Consequently, the thickness of this layer significantly influences the diffusion of blood gases like CO_2 [110]. Studies have shown that the thickness of stratum corneum can vary among individuals depending on the factors like pigmentation and smoking habits [111], [112]. Hence, it is crucial to account for these individual differences when estimating $PaCO_2$ from $PtcCO_2$ and to integrate the impact of such factors into the estimation algorithm.

Such algorithms can be developed based on computational physiological modelling [113]. Recent research employed a simplified adaptation of Krogh's model [114] to simulate the transport of transcutaneous O_2, relating different properties of skin such as thickness and porosity with the O_2 transport, with the aim of accommodating variations within and between individuals [115]. These models have the potential to be modified for transcutaneous CO_2 transport, serving as a foundation for the development of more intricate models tailored to provide personalized predictions for estimating $PaCO_2$ from $PtcCO_2$.

H. Ease of Use

To enable users to utilize $PtcCO_2$ monitors in home-care settings from a distance, it is important to ensure that these monitors are easy to use and maintain. The electrochemical-based monitors require the replacement of their sensing membrane every 28 days by trained personnel [23]. However, if the sensor is regularly cleaned and disinfected, this time frame can be extended to 42 days. The CO_2-sensitive film used in luminescence-based monitors must also be regularly replaced, however, the specific frequency of replacement depends on the excitation scheme employed [39]. Regular maintenance is not reported for NDIR-based monitors as they do not utilize any chemical components that deteriorate in performance over time [25], [26].

Transcutaneous CO_2 monitoring outside of a clinical setting could benefit patients with respiratory diseases. This application requires wearable monitors that are small, comfortable, and accurate with fast response times and low power consumption. Although electrochemical-based $PtcCO_2$ monitors have shown accuracy in clinical tests [9], [22], [95], [96], [97], they were not originally designed for wearable use but for clinical bedside monitoring. NDIR-based monitors can operate for long periods without calibration, but increasing their measurement sensitivity requires larger measurement cells; thus, they need to be miniaturized, which is a challenge. Luminescence-based $PtcCO_2$ monitors, despite their smaller sensor size and fast response time, suffer from photobleaching of the sensing film, limiting continuous measurement time that could be improved by decreasing the sampling rate. In general, the initial settlement time of $PtcCO_2$ monitors is slowed down due to the time required for the CO_2 concentration in the measurement medium to reach equilibrium, which is a function of the diffusion rate of CO_2 through skin. Nevertheless, it is important to highlight that NDIR- and luminescence-based monitors, without heating, exhibit comparable initial settlement times to electrochemical-based monitors that employ a heating element.

VI. Conclusion

An unmet need for a miniaturized, wearable, long-term, and continuous monitoring device that can track $PtcCO_2$ outside a clinical setting remains. Therefore, this article provided a comprehensive review of general sensing techniques and implementation approaches for transcutaneous CO_2 monitoring. To provide the reader with the fundamental concepts of these techniques, we discussed three sensing approaches–electrochemical-, NDIR-, and luminescence-based methods–currently employed in transcutaneous CO_2 monitors. We categorized contemporary and emerging transcutaneous monitors based on their sensing principles and examined them in depth. As contemporary monitors that use electrochemical sensing are designed for clinical use as bedside monitors, researchers have turned to recent developments in sensing technologies to propose alternatives to the contemporary monitors, namely NDIR- and luminescence-based monitors. Our review has demonstrated that these monitors address some of the issues of contemporary monitors and offer promising solutions.

References

[1] S. M. Levine and D. D. Marciniuk, "Global impact of respiratory disease: What can we do, together, to make a difference?," *Chest*, vol. 161, no. 5, pp. 1153–1154, 2022.

[2] "Who coronavirus (COVID-19) dashboard." Accessed: May, 2023. [Online]. Available: https://covid19.who.int/

[3] "Most recent national asthma data," 2021. [Online]. Available: https://www.cdc.gov/asthma/most_recent_national_asthma_data.htm

[4] E. P. Trulock, "Arterial Blood Gases," in *Clinical Methods: The History, Physical, and Laboratory Examinations*, 3rd ed., H. K. Walker et al., Eds. Boston, MA, USA: Butterworths, 1990.

[5] Z. Messina and H. Patrick, *Partial Pressure of Carbon Dioxide* Treasure Island, FL, USA: StatPearls Publishing, 2022.

[6] E. Zeserson et al., "Correlation of venous blood gas and pulse oximetry with arterial blood gas in the undifferentiated critically ill patient," *J. Intensive Care Med.*, vol. 33, no. 3, pp. 176–181, Mar. 2018.

[7] A. Goenka et al., "Neonatal blood gas sampling methods," *South Afr. J. Child Health*, vol. 6, no. 1, pp. 1–18, 2012.

[8] R. T. Brouillette and D. H. Waxman, "Evaluation of the newborn's blood gas status, National academy of clinical biochemistry," *Clin. Chem.*, vol. 43, no. 1, pp. 215–221, Jan. 1997.

[9] J. H. Storre et al., "Transcutaneous monitoring as a replacement for arterial PCO_2 monitoring during nocturnal non-invasive ventilation," *Respir. Med.*, vol. 105, no. 1, pp. 143–150, Jan. 2011.

[10] J. D. Tobias, "Transcutaneous carbon dioxide monitoring in infants and children," *Pediatr. Anesth.*, vol. 19, no. 5, pp. 434–444, 2009.

[11] M. Folke et al., "Critical review of non-invasive respiratory monitoring in medical care," *Med. Biol. Eng. Comput.*, vol. 41, no. 4, pp. 377–383, Jul. 2003.

[12] I. Costanzo, D. Sen, L. Rhein, and U. Guler, "Respiratory monitoring: Current state of the art and future roads," *IEEE Rev. Biomed. Eng.*, vol. 15, pp. 103–121, 2022.

[13] S. E. Huttmann et al., "Techniques for the measurement and monitoring of carbon dioxide in the blood," *Ann. Amer. Thoracic Soc.*, vol. 11, no. 4, pp. 645–652, Apr. 2014.

[14] K. M. Miller et al., "Long-term tolerability of capnography and respiratory inductance plethysmography for respiratory monitoring in pediatric patients treated with patient-controlled analgesia," *Pediatr. Anesth.*, vol. 25, no. 10, pp. 1054–1059, Oct. 2015.

[15] T. Enomoto et al., "Limitations of end-tidal CO_2 measured with a portable capnometer to estimate $PaCO_2$ for patients with respiratory disease," *Turkish Thoracic J.*, vol. 22, no. 3, pp. 212–216, Jun. 2021.

[16] M. Dicembrino et al., "End-tidal CO_2 and transcutaneous CO_2: Are we ready to replace arterial CO_2 in awake children?," *Pediatr. Pulmonol.*, vol. 56, no. 2, pp. 486–494, 2021.

[17] K. P. Sullivan et al., "Transcutaneous carbon dioxide pattern and trend over time in preterm infants," *Pediatr. Res.*, vol. 90, pp. 840–846, Jan. 2021.

[18] J. Carrington et al., "Transcutaneous carbon dioxide monitoring could reduce physical contact with COVID-19 patients," *Amer. J. Hosp. Med.*, vol. 5, no. 3, pp. 1–6, Sep. 2021.

[19] J. W. Severinghaus and A. Freeman, "Electrodes for blood pO2, and pCO_2, determination," *J. App. Physiol.*, vol. 13, no. 3, pp. 515–520, 1958.

[20] J. W. Severinghaus, "A combined transcutaneous PO_2-PCO_2 electrode with electrochemical HCO_3- stabilization," *J. Appl. Physiol.*, vol. 51, no. 4, pp. 1027–1032, Oct. 1981.

[21] P. N. Chhajed et al., "Infraclavicular sensor site: A new promising site for transcutaneous capnography," *Scand. J. Clin. Lab. Investigation*, vol. 72, no. 4, pp. 340–342, Jul. 2012.

[22] A. K. Bhalla et al., "Accuracy of transcutaneous carbon dioxide levels in comparison to arterial carbon dioxide levels in critically ill children," *Respir. Care*, vol. 64, no. 2, pp. 201–208, Feb. 2019.

[23] *Technical Manual for Sentec Digital Monitor*, Therwil, Switzerland: Sentec AG, 2021. [Online]. Available: https://www.sentec.com/fileadmin/documents/Labeling/Technical_Manuals/HB-005752-t-SDM_Technical_Manual.pdf

[24] J. Nagler and B. Krauss, "Capnography: A valuable tool for airway management," *Emerg. Med. Clin. North Amer.*, vol. 26, no. 4, pp. 881–897, Nov. 2008.

[25] P. Grangeat et al., "First evaluation of a transcutaneous carbon dioxide monitoring wristband device during a cardiopulmonary exercise test," in *Proc. IEEE 41st Annu. Int. Conf. Eng. Med. Biol. Soc.*, 2019, pp. 3352–3355.

[26] V. V. Tipparaju et al., "Wearable transcutaneous CO_2 monitor based on miniaturized nondispersive infrared sensor," *IEEE Sensors J.*, vol. 21, no. 15, pp. 17327–17334, Aug. 2021.

[27] T. B. Tufan and U. Guler, "A fluorescent thin film-based miniaturized transcutaneous carbon dioxide monitor," in *Proc. IEEE Biomed. Circuits Syst. Conf.*, 2021, pp. 1–5.

[28] J. P. Cascales et al., "A patient-ready wearable transcutaneous CO_2 sensor," *Biosensors*, vol. 12, no. 5, May 2022, Art. no. 333.

[29] T. B. Tufan and U. Guler, "A miniaturized transcutaneous carbon dioxide monitor based on dual lifetime referencing," in *Proc. IEEE Biomed. Circuits Syst. Conf.*, 2022, pp. 144–148.

[30] C. Higgins, "Why measure blood gases? A three-part introduction for the novice - Part 1," p. 9, Jan. 2012. [Online]. Available: https://acutecaretesting.org/en/articles/why-measure-blood-gases-a-three-part-introduction-for-the-novice-part-2

[31] C. Higgins, "Why measure blood gases? A three-part introduction for the novice - Part 2," p. 9, Apr. 2012. [Online]. Available: https://acutecaretesting.org/en/articles/why-measure-blood-gases-a-three-part-introduction-for-the-novice-part-2

[32] R. Krapf, "Hypo- and hyperventilation: Consequences for acid-base balance," *Schweizerische Rundschau Fur Medizin Praxis*, vol. 80, no. 40, pp. 1058–1061, Oct. 1991.

[33] E. Hopkins et al., *Physiology, Acid Base Balance*. Treasure Island, FL, USA: StatPearls Publishing, 2022.

[34] C. Dave et al., "Development and relevance of hypercapnia in COPD," *Can. Respir. J.*, vol. 2021, Feb. 2021, Art. no. 6623093.

[35] Y. Mendelson and R. A. Peura, "Noninvasive transcutaneous monitoring of arterial blood gases," *IEEE Trans. Biomed. Eng.*, vol. BME-31, no. 12, pp. 792–800, Dec. 1984.

[36] *Sentec Transcutaneous Monitoring System*. Therwil, Switzerland: Sentec AG. Accessed: May, 2023. [Online]. Available: https://www.sentec.com/transcutaneous-monitoring/

[37] G. F. Curley et al., "Hypocapnia and hypercapnia," in *Murray and Nadel's Textbook of Respiratory Medicine*. Amsterdam, The Netherlands: Elsevier, 2016, pp. 1527–1546.

[38] D. Sankaran et al., "Non-invasive carbon dioxide monitoring in neonates: Methods, benefits, and pitfalls," *J. Perinatol.*, vol. 41, pp. 2580–2589, Jun. 2021.

[39] T. B. Tufan and U. Guler, "A transcutaneous carbon dioxide monitor based on time-domain dual lifetime referencing," *IEEE Trans. Biomed. Circuits Syst.*, vol. 17, no. 4, pp. 795–807, Aug. 2023, doi: 10.1109/TBCAS.2023.3277398..

[40] P. Zhao and W.-J. Cai, "An improved potentiometric pCO_2 microelectrode," *Anal. Chem.*, vol. 69, no. 24, pp. 5052–5058, Dec. 1997.

[41] J. Severinghaus, "The invention and development of blood gas analysis apparatus," *Anesthesiology*, vol. 97, no. 1, pp. 253–256, Jul. 2002.

[42] R. W. Stow et al., "Rapid measurement of the tension of carbon dioxide in the blood," *Archieves Phys. Med. Rehabil.*, vol. 38, no. 10, pp. 646–650, Oct. 1957.

[43] J. W. Severinghaus, "Methods of measurement of blood and gas carbon dioxide during anesthesia," *Anesthesiology*, vol. 21, pp. 717–726, Dec. 1960.

[44] C. R. Caflisch and N. W. Carter, "A micro pCO_2 electrode," *Anal. Biochem.*, vol. 60, no. 1, pp. 252–257, Jul. 1974.

[45] H. Beyenal et al., "An improved Severinghaus-type carbon dioxide microelectrode for use in biofilms," *Sensors Actuators B: Chem.*, vol. 97, no. 2/3, pp. 202–210, Feb. 2004.

[46] W. van Weteringen et al., "Novel transcutaneous sensor combining optical $tcPO_2$ and electrochemical $tcPCO_2$ monitoring with reflectance pulse oximetry," *Med. Biol. Eng. Comput.*, vol. 58, no. 2, pp. 239–247, Nov. 2019.

[47] M. Xu et al., "Multi-gas detection system based on non-dispersive infrared (NDIR) spectral technology," *Sensors*, vol. 22, no. 3, Jan. 2022, Art. no. 836.

[48] L. Zhou et al., "Carbon dioxide sensor module based on NDIR technology," *Micromachines*, vol. 12, no. 7, Jul. 2021, Art. no. 845.

[49] P. Grangeat et al., "Evaluation in healthy subjects of a transcutaneous carbon dioxide monitoring wristband during hypo and hypercapnia conditions," in *Proc. IEEE 42nd Annu. Int. Conf. Eng. Med. Biol. Soc.*, 2020, pp. 4640–4643.

[50] L. Scholz et al., "Carbon dioxide sensor for mobile devices: A novel approach for low-power consuming, highly sensitive NDIR sensors," in *Proc. IEEE Sensors*, 2016, pp. 1–3.

[51] R. K. Jha, "Non-dispersive infrared gas sensing technology: A review," *IEEE Sensors J.*, vol. 22, no. 1, pp. 6–15, Jan. 2021.

[52] S. Palzer, "Photoacoustic-based gas sensing: A review," *Sensors*, vol. 20, no. 9, May 2020, Art. no. 2745.

[53] T. Vincent and J. Gardner, "A low cost MEMS based NDIR system for the monitoring of carbon dioxide in breath analysis at PPM levels," *Sensors Actuators B: Chem.*, vol. 236, pp. 954–964, Nov. 2016.

[54] Q. Tan et al., "Three-gas detection system with IR optical sensor based on NDIR technology," *Opt. Lasers Eng.*, vol. 74, pp. 103–108, Nov. 2015.

[55] J. R. Lakowicz, *Principles of Fluorescence Spectroscopy*, 3rd ed. New York, NT, USA: Springer, 2006.

[56] P. K. Contreras-Gutierrez et al., "A new highly sensitive and versatile optical sensing film for controlling CO_2 in gaseous and aqueous media," *Sensors Actuators B: Chem.*, vol. 184, pp. 281–287, Jul. 2013.

[57] D. Atamanchuk et al., "Performance of a lifetime-based optode for measuring partial pressure of carbon dioxide in natural waters," *Limnol. Oceanogr.: Methods*, vol. 12, no. 2, pp. 63–73, 2014.

[58] M. Čajlaković et al., "Luminescence lifetime-based carbon dioxide optical sensor for clinical applications," *Analytica Chimica Acta*, vol. 573–574, pp. 57–64, Jul. 2006.

[59] Z. Hetzler et al., "Flexible sensor patch for continuous carbon dioxide monitoring," *Front. Chem.*, vol. 10, Sep. 2022, Art. no. 983523.

[60] I. Costanzo et al., "A noninvasive miniaturized transcutaneous oxygen monitor," *IEEE Trans. Biomed. Circuits Syst.*, vol. 15, no. 3, pp. 474–485, Jun. 2021.

[61] H. Szmacinski and J. R. Lakowicz, "Optical measurements of pH using fluorescence lifetimes and phase-modulation fluorometry," *Anal. Chem.*, vol. 65, no. 13, pp. 1668–1674, Jul. 1993.

[62] D. J. S. Birch and R. E. Imhof, "Time-domain fluorescence spectroscopy using time-correlated single-photon counting," in *Topics in Fluorescence Spectroscopy*, J. R. Lakowicz, Ed., vol. 1. Boston, MA, USA: Kluwer Academic Publishers, 2002, pp. 1–95.

[63] K. Santra et al., "Photon counting data analysis: Application of the maximum likelihood and related methods for the determination of lifetimes in mixtures of rose Bengal and rhodamine B," *J. Phys. Chem. A*, vol. 121, no. 1, pp. 122–132, Jan. 2017.

[64] A. Bitton et al., "A review of new high-throughput methods designed for fluorescence lifetime sensing from cells and tissues," *Front. Phys.*, vol. 9, Apr. 2021, Art. no. 648553.

[65] P. Kapusta et al. Eds., *Advanced Photon Counting: Applications, Methods, Instrumentation*, vol. 15. Cham, Switzerland: Springer Int. Publishing, 2015.

[66] J. P. V. S. Cunha, M. Begalli, and M. D. Bellar, "High voltage power supply with low power consumption for photomultiplier tubes," in *Proc. IEEE Nucl. Sci. Symp. Med. Imag. Conf.*, 2010, pp. 1354–1357.

[67] Y. Tian et al., "Low detection limit time-correlated single photon counting lifetime analytical system for point-of-care applications," *IEEE Access*, vol. 7, pp. 18256–18266, 2019.

[68] D. Tamborini et al., "Compact, low-power and fully reconfigurable 10 ps resolution, 160 μs range, time-resolved single-photon counting system," *IEEE Sensors J.*, vol. 16, no. 10, pp. 3827–3833, May 2016.

[69] S. P. Chan et al., "New method of rapid luminescence lifetime determination using square-wave excitation," *Appl. Spectrosc.*, vol. 55, no. 9, pp. 1245–1250, Sep. 2001.

[70] S. P. Chan et al., "Optimized gating scheme for rapid lifetime determinations of single-exponential luminescence lifetimes," *Anal. Chem.*, vol. 73, no. 18, pp. 4486–4490, Sep. 2001.

[71] I. Costanzo et al., "A nonuniform sampling lifetime estimation technique for luminescent oxygen measurements," in *Proc IEEE 48th Eur. Solid State Circuits Conf.*, 2022, pp. 413–416.

[72] T. B. Tufan et al., "Performance analysis of a flexible HPTS-Based carbon dioxide sensor for transcutaneous blood gas monitoring," in *Proc. IEEE Biomed. Circuits Syst. Conf.*, 2023, pp. 1–5.

[73] I. Klimant et al., "Dual Lifetime Referencing (DLR) – a New Scheme for Converting Fluorescence Intensity into a Frequency-Domain or Time-Domain Information," in *New Trends in Fluorescence Spectroscopy: Applications to Chemical and Life Sciences*, B. Valeur and J.-C. Brochon, Eds. Berlin, Heidelberg: Springer, 2001, pp. 257–274.

[74] I. Klimant, "Method and device for referencing fluorescence intensity signals," U.S. Patent 6602716B1, Aug. 05, 2003.

[75] J. S. Clarke et al., "Characterization of a time-domain dual lifetime referencing pCO_2 optode and deployment as a high-resolution underway sensor across the high latitude North Atlantic Ocean," *Front. Mar. Sci.*, vol. 4, 2017, Art. no. 396.

[76] G. Liebsch et al., "Fluorescent imaging of pH with optical sensors using time domain dual lifetime referencing," *Anal. Chem.*, vol. 73, no. 17, pp. 4354–4363, Sep. 2001.

[77] C. Huber et al., "Dual lifetime referencing as applied to a chloride optical sensor," *Anal. Chem.*, vol. 73, no. 9, pp. 2097–2103, May 2001.

[78] L. Ding et al., "Long-term quantitatively imaging intracellular chloride concentration using a core-/shell-structured nanosensor and time-domain dual-lifetime referencing method," *ACS Sensors*, vol. 5, no. 12, pp. 3971–3978, Dec. 2020.

[79] E. Berardesca and H. Maibach, "Transcutaneous CO_2 and O_2 diffusion," *Skin Pharmacol. Physiol.*, vol. 6, pp. 3–9, 1993.

[80] P. D. Wimberley et al., "Transcutaneous carbon dioxide and oxygen tension measured at different temperatures in healthy adults," *Clin. Chem.*, vol. 31, no. 10, pp. 1611–1615, Oct. 1985.

[81] E. Dervieux et al., "Carbon dioxide sensing–biomedical applications to human subjects," *Sensors*, vol. 22, no. 1, Dec. 2021, Art. no. 188.

[82] H.-J. Lee et al., "Development of non-invasive optical transcutaneous pCO/sub 2/ gas sensor and analytic equipment," in *Proc. IEEE Sensors*, 2004, pp. 730–733.

[83] R. Frodl and T. Tille, "A high-precision NDIR CO_2 gas sensor for automotive applications," *IEEE Sensors J.*, vol. 6, no. 6, pp. 1697–1705, Dec. 2006.

[84] S. Yi et al., "Novel NDIR CO_2 sensor for indoor air quality monitoring," in *Proc. IEEE 13th Int. Conf. Solid-State Sensors, Actuators Microsystems. Dig. Tech. Papers. Transducers*, 2005, pp. 1211–1214.

[85] T. B. Tufan, D. Sen, and U. Guler, "An infra-red-based prototype for a miniaturized transcutaneous carbon dioxide monitor," in *Proc. IEEE 43rd Annu. Int. Conf. Eng. Med. Biol. Soc.*, 2021, pp. 7132–7135.

[86] M. Chatterjee et al., "A rate-based transcutaneous CO_2 sensor for noninvasive respiration monitoring," *Physiol. Meas.*, vol. 36, no. 5, pp. 883–894, May 2015.

[87] D. Rudmann et al., "Sensor for detection of gas and method for detection of gas," U.S. Patent 10,307,090, Jun. 04, 2019.

[88] R. Lee and W. Kester, "Complete gas sensor circuit using nondispersive infrared (NDIR)," *Analog Dialogue*, vol. 50, pp. 1–9, 2016.

[89] S. F. Silva et al., "Can we use rapid lifetime determination for fast, fluorescence lifetime based, metabolic imaging? Precision and accuracy of double-exponential decay measurements with low total counts," *PLoS One*, vol. 14, no. 5, May 2019, Art. no. e0216894.

[90] R. N. Dansby-Sparks et al., "Fluorescent-dye-doped sol-gel sensor for highly sensitive carbon dioxide gas detection below atmospheric concentrations," *Anal. Chem.*, vol. 82, no. 2, pp. 593–600, Jan. 2010.

[91] Y. Amao and T. Komori, "Optical CO_2 sensor of the combination of colorimetric change of α-naphtholphthalein in poly (isobutyl methacrylate) and fluorescent porphyrin in polystyrene," *Talanta*, vol. 66, no. 4, pp. 976–981, May 2005.

[92] C.-S. Chu and J.-J. Syu, "Optical sensor for dual sensing of oxygen and carbon dioxide based on sensing films coated on filter paper," *Appl. Opt.*, vol. 56, no. 4, Feb. 2017, Art. no. 1225.

[93] *TCM TOSCA/CombiM Operator's Manual*. Bronshoj, Denmark: Radiometer Medical ApS, 2011.

[94] X. Ge et al., "Development and characterization of a point-of care rate-based transcutaneous respiratory status monitor," *Med. Eng. Phys.*, vol. 56, pp. 36–41, Jun. 2018.

[95] P. Chaudhari et al., "VentCheck: Spot measurement of combined oximetry & cutaneous carbon dioxide to screen for type II respiratory failure in respiratory illness," *Eur. Respir. J.*, vol. 38, no. Suppl 55, p. p907, Sep. 2011.

[96] C. Horvath et al., "Real-time measurement of transcutaneous PCO_2 vs arterial/venous PCO_2 in subjects with severe respiratory failure undergoing non-invasive ventilation on the emergency department–An observational study," *Eur. Respir. J.*, vol. 46, Sep. 2015, Art. no. OA503.

[97] W. van Weteringen et al., "Validation of a new transcutaneous $tcPO_2$/$tcPCO_2$ sensor with an optical oxygen measurement in preterm neonates," *Neonatology*, vol. 117, no. 5, pp. 628–636, 2020.

[98] D. E. Kim et al., "Noninvasive optical transcutaneous pCO_2 gas sensor," *Sensors Mater.*, vol. 17, no. 5, pp. 249–257, 2005.

[99] V. Vakhter et al., "A prototype wearable device for noninvasive monitoring of transcutaneous oxygen," *IEEE Trans. Biomed. Circuits Syst.*, vol. 17, no. 2, pp. 323–335, Apr. 2023.

[100] M. Wahl, "Modern TCSPC electronics: Principles and acquisition modes," in *Advanced Photon Counting: Applications, Methods, Instrumentation*, P. Kapusta et al., Eds. Cham, Switzerland: Springer Int. Publishing, 2015, pp. 1–21.

[101] "What is MPPC (SIPM)?: Multi-pixel photon counters (MPPCS/SIPMS)." Accessed: Apr., 2023. [Online]. Available: https://www.hamamatsu.com/us/en/product/optical-sensors/mppc/what_is_mppc/index.html

[102] N. A. W. Dutton et al., "11.5 a time-correlated single-photon-counting sensor with 14GS/S histogramming time-to-digital converter," in *Proc. IEEE Int. Solid-State Circuits Conf. Dig. Tech. Papers*, 2015, pp. 1–3.

[103] R. Scott, W. Jiang, and M. J. Deen, "CMOS time-to-digital converters for biomedical imaging applications," *IEEE Rev. Biomed. Eng.*, vol. 16, pp. 627–652, 2023.

[104] A. T. Erdogan et al., "A high dynamic range 128 $\times$ 120 3-D stacked CMOS SPAD image sensor SoC for fluorescence microendoscopy," *IEEE J. Solid-State Circuits*, vol. 57, no. 6, pp. 1649–1660, Jun. 2022.

[105] U. Guler et al., "Sensors for neonatal monitoring," in *Encyclopedia of Sensors and Biosensors*, 1st ed, R. Narayan, Ed., Amsterdam, The Netherlands: Elsevier, 2022, pp. 423–448.

[106] "Cutaneous carbon dioxide ($PcCO_2$) and oxygen (PcO_2) monitors - class II special controls guidance document for industry and FDA," *U.S. Dept. Health Human Serv.*, Dec. 2002.

[107] O. Such, "Motion tolerance in wearable sensors–The challenge of motion artifact," in *Proc. IEEE 29th Annu. Int. Conf. Eng. Med. Biol. Soc.*, 2007, pp. 1542–1545.

[108] V. Vakhter et al., "The impact of motion artifacts on transcutaneous oxygen measurements," in *Proc. IEEE Biomed. Circuits Syst. Conf.*, 2023, pp. 1–5.

[109] H. Lee, H. Chung, and J. Lee, "Motion artifact cancellation in wearable photoplethysmography using gyroscope," *IEEE Sensors J.*, vol. 19, no. 3, pp. 1166–1175, Feb. 2019.

[110] M. E. Hatcher and W. Z. Plachy, "Dioxygen diffusion in the stratum corneum: An EPR spin label study," *Biochimica et Biophysica Acta (BBA) - Biomembranes*, vol. 1149, no. 1, pp. 73–78, Jun. 1993.

[111] K. A. Holbrook and G. F. Odland, "Regional differences in the thickness (cell layers) of the human stratum corneum: An ultrastructural analysis," *J. Invest. Dermatol.*, vol. 62, no. 4, pp. 415–422, Apr. 1974.

[112] J. Sandby-Møller et al., "Epidermal thickness at different body sites: Relationship to age, gender, pigmentation, blood content, skin type and smoking habits," *Acta Dermato-Venereologica*, vol. 83, no. 6, pp. 410–413, 2003.

[113] R. S. P. Warnaar et al., "Computational physiological models for individualised mechanical ventilation: A systematic literature review focussing on quality, availability, and clinical readiness," *Crit. Care*, vol. 27, no. 1, Jul. 2023, Art. no. 268.

[114] A. S. Popel, "Theory of oxygen transport to tissue," *Crit. Rev. Biomed. Eng.*, vol. 17, no. 3, pp. 257–321, 1989.

[115] D. Sen et al., "Poster: Towards hardware and software integration of noninvasive transcutaneous oxygen monitor," in *Proc. IEEE/ACM Conf. Connected Health: Appl., Syst. Eng. Technol.*, 2022, pp. 156–157.